The EPIC pn-CCD detector aboard XMM-Newton: status of the background calibration

Michael J. Freyberg[a], Ulrich G. Briel[a], Konrad Dennerl[a], Frank Haberl[a], Gisela Hartner[a], Elmar Pfeffermann[a], Eckhard Kendziorra[b], Marcus Kirsch[c], and David Lumb[d]

[a] Max-Planck-Institut für extraterrestrische Physik, Giessenbachstraße, 85740 Garching, Germany

[b] Institut für Astronomie und Astrophysik der Universität Tübingen, Abteilung Astronomie, Sand 1, 72076 Tübingen, Germany

[c] ESA RSSD SCI-SD, XMM-Newton SOC Vilspa, Apartado - P.O. Box 50727, 28080 Madrid, Spain

[d] ESA SPTD RSSD, ESTEC, Postbus 299, Keplerlaan 1, Noordwijk, The Netherlands

ABSTRACT

We report on the current status of the background calibration of the EPIC pn-CCD camera on board XMM-Newton. The intrinsic background is comprised of internal electronic noise, and continuous and fluorescent X-ray emission induced by high-energy particles. Soft protons passing through the X-ray telescope (and finally also true cosmic X-rays) contribute to the registered events. The camera background has been monitored by using data in closed filter positions for three years; we review the spectral, spatial, and temporal distribution, for all commissioned instrument modes. This paper also discusses briefly the effects on scientific data analysis and conclusions for further observations and detectors.

Keywords: XMM-Newton, EPIC, pn-CCD, X-ray detector, X-ray calibration, fluorescence lines

1. INTRODUCTION

The in-orbit performance[1] of the *European Photon Imaging Camera* (EPIC) pn-CCD detector[2] (consisting of 12 CCDs on a monolithic wafer) aboard XMM-Newton[3] is monitored by observations of dedicated astrophysical objects[4] (like supernova remnants, isolated neutron stars, BL Lac objects) as well as by exposures using the filter wheel in "Closed" and "CalClosed" positions.[5,6] The EPIC-pn camera can be operated in several instrument modes[2] with a variety of integration times and readout schemes depending on the scientific needs of the astrophysical target. The camera background is different for all these modes: full frame (FF), extended full frame (eFF), large window (LW), small window (SW), timing (TI), and burst (BU) modes.

Closed filter data are used to analyse the internal camera background over the whole available energy range ($0.1 - 30\,\mathrm{keV}$) without significant contribution by cosmic X-rays or energetic particles passing through the telescope. When turning the EPIC-pn filter wheel[5] by a few degrees a radioactive ^{55}Fe calibration source can illuminate almost the full sensitive CCD area through a hole in the filter wheel (*CalClosed* position). These exposures serve as monitor of the spectral response of EPIC-pn. Above the highest energy of this internal calibration source (i.e. the Mn-Kβ line at $\sim 6.4\,\mathrm{keV}$) these data are also used to investigate spatial, spectral, and temporal properties of the detector background. We like to note that this filter position is often realized when no scientific observations can be performed due to high radiation: these extra charges can increase the charge transfer efficiency[7] (CTE) by saturation of traps and thus shifted line positions, therefore some of the "calibration" observations are unsuited for calibration purposes.

Due to the large pixel size of $150\,\mu\mathrm{m} \times 150\,\mu\mathrm{m}$ only a few pixels can receive charges induced by an individual photon. Depending on the size of such an event pixel pattern these events are classified as "singles", "doubles", "triples", and "quadruple" events[7] (any larger pattern size is due to pattern pile-up and cannot be produced by a single photon; those events are usually discarded from a scientific analysis). This split event behaviour depends e.g. on photon energy, detector position, and instrument mode. As will be shown later these pattern fractions are different for internal camera background X-rays and for X-rays that have passed through the

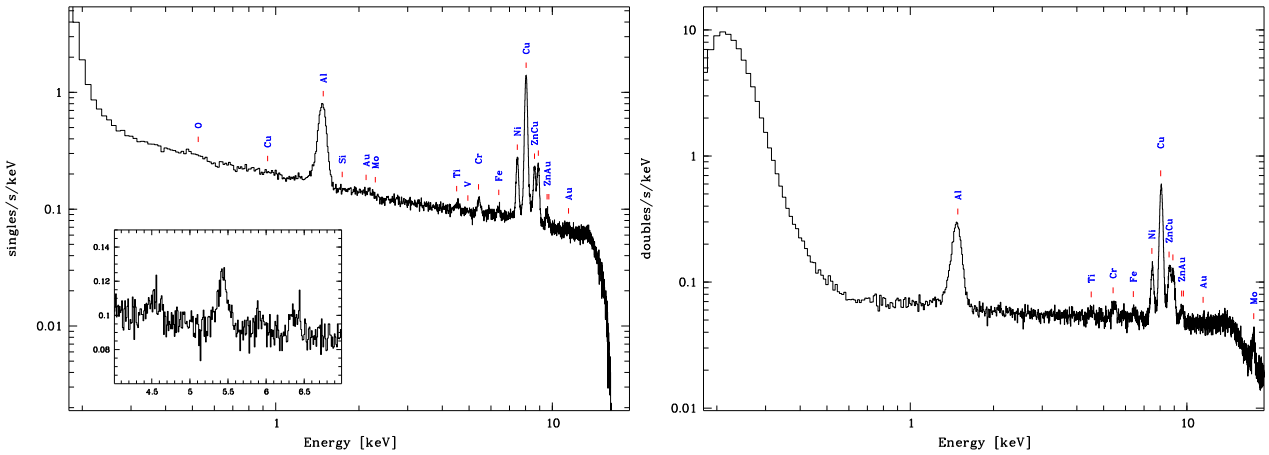

Figure 1. EPIC-pn spectra ($0.2-18$ keV) of the full detector area using the "Closed" filter observations in full frame modes (FF+eFF) taken during the first 3 years in orbit (313 ks), in single-pixel events (left) and double-pixel events (right). Several prominent features are seen (e.g., Al-Kα, Ni-Kα, and Cu-Kα lines). The insert is a close-up of the spectral range $4-7$ keV where a few weak features can be seen. Note also the Mo-Kα line at 17.4 keV which is only visible in the doubles due to the onboard MIP rejection threshold2 which suppresses individual events above 15 keV. The different spectral continuum slope is due to the energy dependence of the single/double ratio (see also Fig.5).

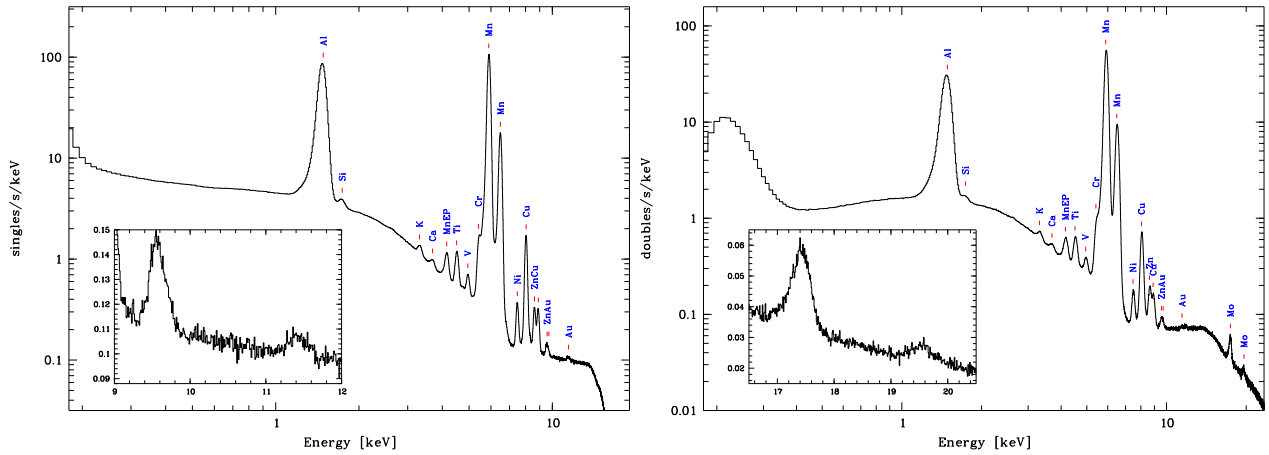

Figure 2. EPIC-pn spectra ($0.2-18$ keV) of the full detector area using the "CalClosed"filter observations in full frame modes (FF+eFF) taken during the first 3 years in orbit (2031 ks), in single-pixel events (left) and double-pixel events (right). The spectrum is created by the onboard radioactive ^{55}Fe calibration source. Above 7 keV this filter position can also be used to study the internal camera background (see Fig.1).

X-ray telescope.[8] Moreover, only a subset of three-pixel and four-pixel events types can be produced by a single photon, impossible are e.g. three adjacent events in one row or in one column etc. These invalid pattern types can be produced by pattern pile-up of valid events with electronic noise or also by "soft proton flare" radiation, and can result in an apparent loss of flux of an astrophysical X-ray source.

2. GLOBAL SPECTRA

Figure 1 shows spectra of all available filter wheel "Closed" data in nominal instrument setup in Full Frame (FF) and extended Full Frame (eFF) modes taken during the first three years in orbit, with a total integration time of 313 ks. The left panel contains the spectrum of single-pixel events while in the right panel only double-pixel events are used. All events within the field-of-view have been collected. The astrophysically interesting

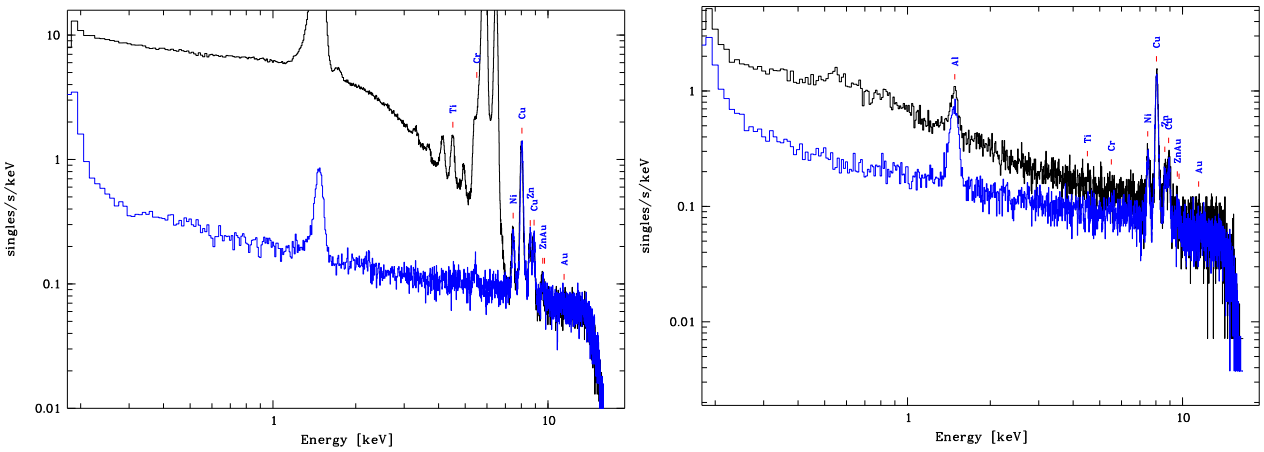

Figure 3. Left: comparison of a FF mode exposure in "CalClosed" filter (top, black) with one in "Closed" filter position (bottom, blue); above 7 keV the spectra agree with each other. Right: comparison of a "blank field" observation[9] (X-ray shadow in Ophiuchus performed with "Thin1" filter) with a "Closed" filter exposure, both in eFF mode; at higher energies the internal background becomes comparable to the sky background.

energy range around the iron K lines is displayed as insert in the left panel, weak features, e.g. at Ti-Kα, Cr-Kα, or Fe-Kα are seen. Note that the noise peak (below 400 eV) differs significantly in singles and doubles, it is broadened as the noise contributes twice to the spectral width.

Similarly, in Fig.2 the spectra of all "CalClosed" observations are shown, with singles (left) and doubles (right panel) separately. Due to the high statistics (total integration time 2031 ks) also weak lines are clearly visible like Au-Lβ (11.4 keV) or the Mo-Kα and Mo-Kβ lines at 17.4 and 19.6 keV (bottom), respectively. It is worth mentioning that the accuracy of the energy corrections in the XMM Standard Analysis Software (XMMSAS) is high so that still outside the X-ray telescope energy band (i.e. above the Au-L edge) the line positions of the high-energy lines differ by less than $< 0.3\%$ from the nominal positions.

Figure 4 illustrates in the left panel the similarity of the high-energy spectrum obtained in "Closed" (bottom, blue) and "CalClosed" (top, black) filter positions. In the right panel a science observation with "Thin1" filter is compared with the "Closed" spectrum observed in the same instrument mode (eFF) just two months later.

3. SPATIAL DISTRIBUTION

Figure 4 illustrates the spatial inhomogeneity of prominent background lines (Ni-Kα, Cu-Kα, Mo-Kα). The Al-Kα line at 1.5 keV appears to be flat. The high-energy lines show striking correspondence with the electronics board mounted below the CCD wafer. Molybdenum is embedded between copper layers, and at the edges of the four individual quadrant plates characteristic line emission can escape. Nickel is correlated with the electronic devices, the CAMEX at the top and bottom, the TIMEX chips, etc. At Ni-K emission enhancements one can observe deficits in the Cu-K emission due to absorption. Zn-K shows a slight increase away from the CAMEX and is also present at the on-axis position. Careful background selection and subtraction is required if one is interested in spectral features close to these inhomogeneous fluorescence lines.

4. MODE DEPENDENCY

In the following we discuss the various "imaging" and "fast" EPIC-pn modes in order of decreasing frame cycle time, from 199.2 ms (eFF) over 73.36 (FF), 47.66 (LW), to 5.67 ms (SW mode), and 5.94 ms (TI) and 4.34 ms (BU mode), respectively. In Figs.5 and 6 the full field-of-view pattern distributions and pattern fractions are shown. Internal background single pixel events appear to be more abundant than the model fractions predict. This is due to "back-side" (actually front-side) illumination of the wafer by radiation from the electronics board excited by high-energetic particles. These secondary X-rays are absorbed close to the front-side and thus have only a short travel distance where the charge cloud could spread - while cosmic X-rays have to traverse the full wafer thickness.

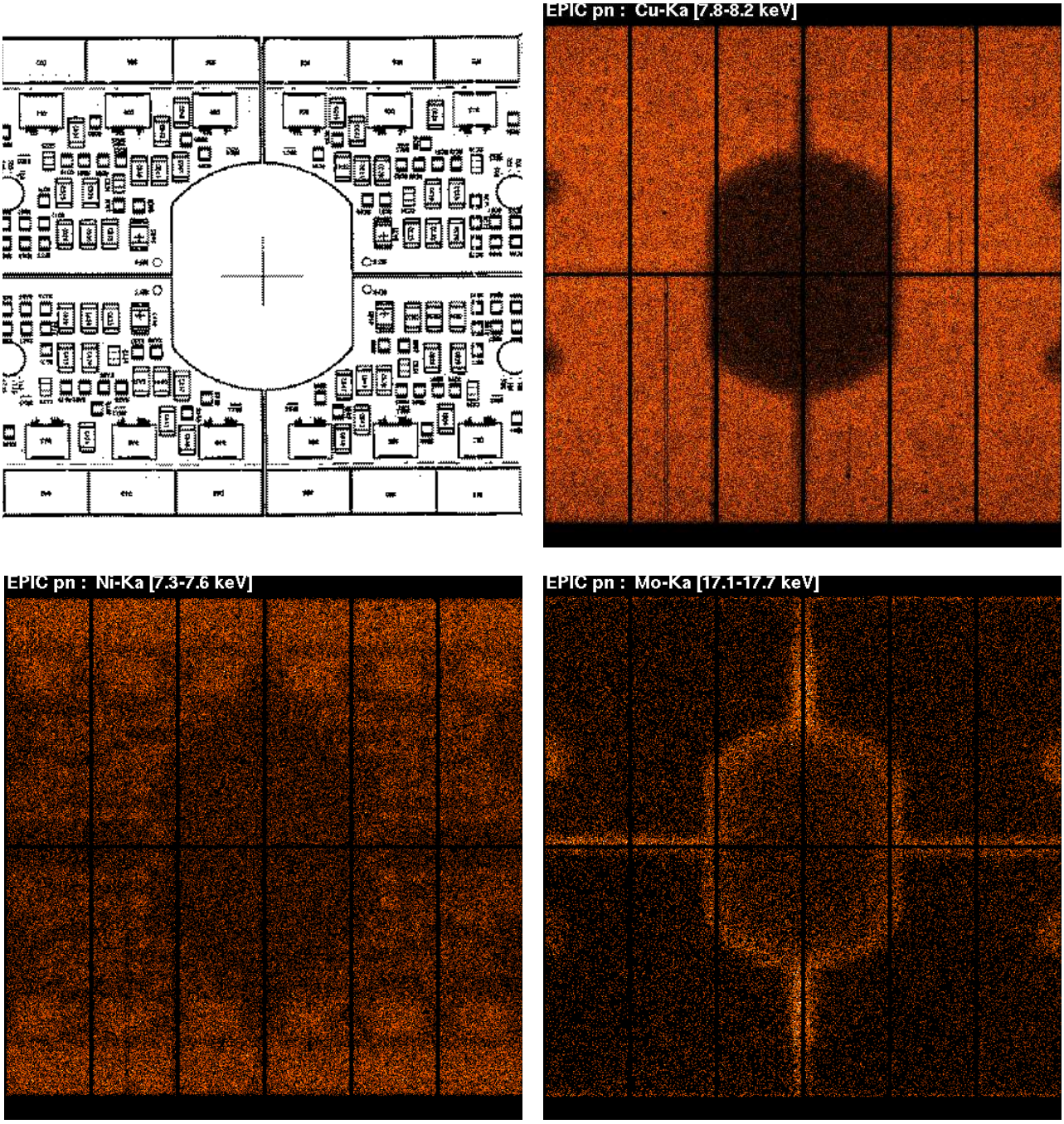

Figure 4. Upper left: layout of the printed circuit board[10] of the EPIC-pn camera, consisting of 4 quadrants with a venting hole in the middle; detector images in narrow energy bands around $K\alpha$ line energies of: (lower left) nickel ($7.3-7.6\,\mathrm{keV}$), (upper right) copper ($7.8-8.2\,\mathrm{keV}$), (lower right) molybdenum ($17.1-17.7\,\mathrm{keV}$). The absolute normalization of the images can be inferred from the spectra (singles, doubles) in Fig. 2. Note that the nominal on-axis position is close to the detector center and thus Cu-K and Ni-K lines are there below average.

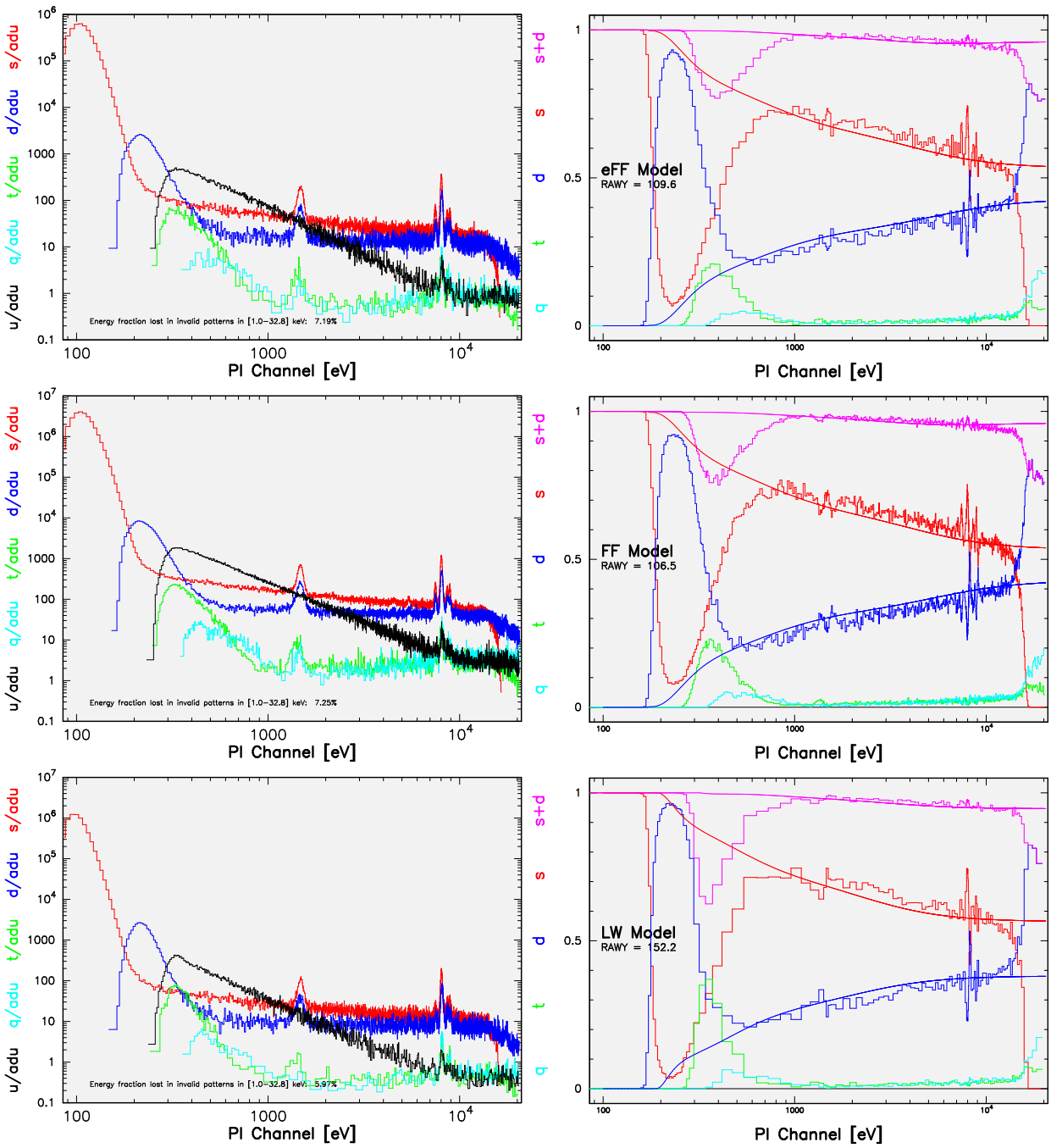

Figure 5. Event pattern distributions (left) and fractions (right panels) for merged eFF, FF, and LW mode "Closed" filter data (from top to bottom), respectively. The lines denote singles (red) starting at 100 eV, doubles (blue) at 200 eV, triples (green) and invalid (black) at 300 eV, and quadruples (turquoise) at 400 eV, as 100 eV is the lower event threshold for all these modes. The solid lines in the right panels indicate the model pattern distributions as function of energy for X-ray photons from the sky for the various modes (along with the "singles + doubles" model in purple colour). Obviously the low-energy noise follows a different split relation, and at higher energies the observed fractions exhibit an increase of single events. As double events collect more noise during readout than single events spectral lines are broadened and the fraction of singles/doubles shows artificial residuals at the core and wing of a line.

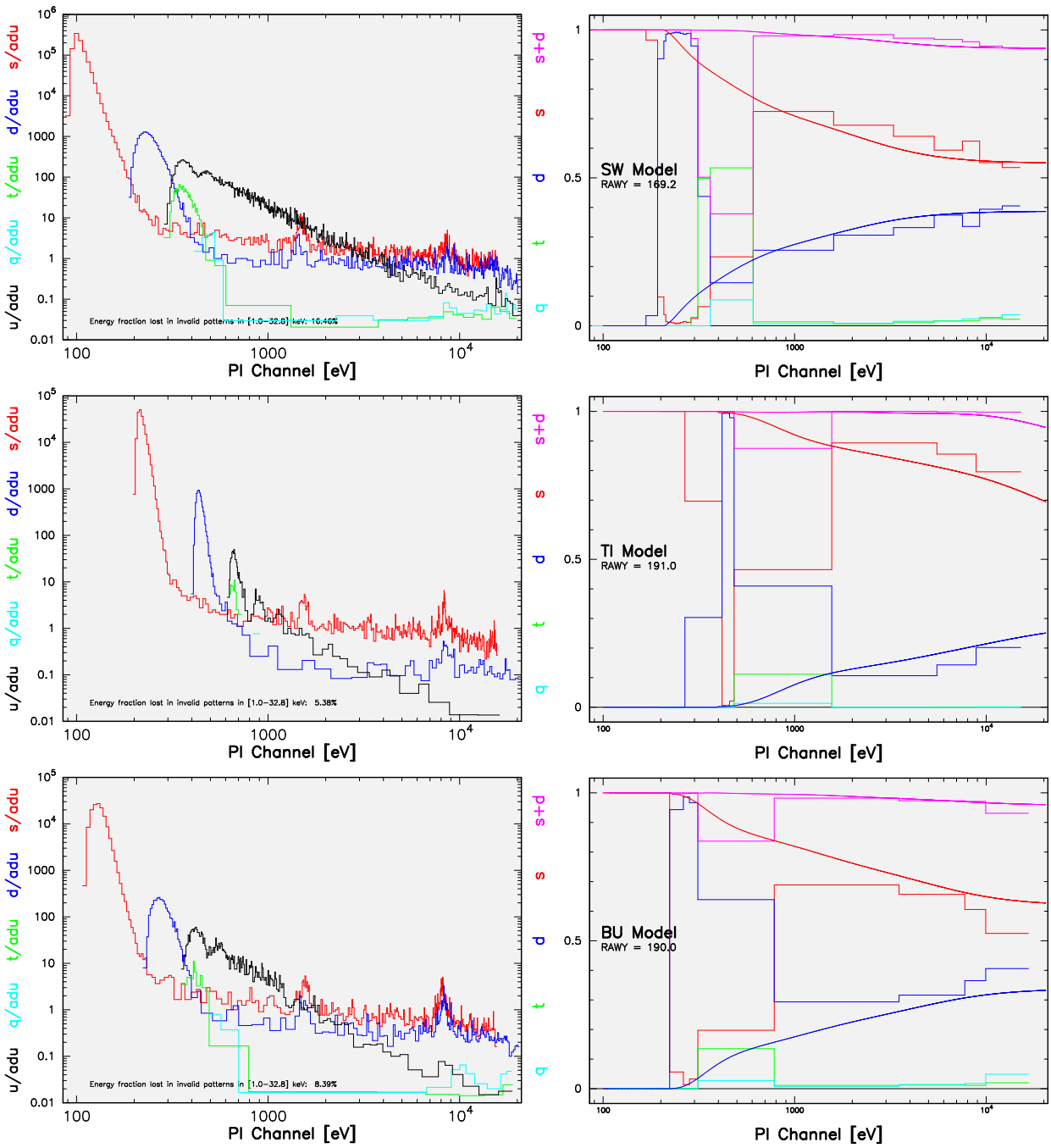

Figure 6. Event pattern distributions (left) and fractions (right) for merged SW, TI, and BU mode "Closed" filter data (from top to bottom), respectively, similar to Fig.5. Note that for TI and BU modes the lower thresholds are about 200 eV and 115 eV, respectively. Due to poorer statistics (smaller CCD area read out as well as lower mode efficiency the pattern fractions (SW, TI modes) show only marginally the trend of increased single event fraction, while in BU mode the model over-predicts the single pattern fraction of the background.

The eFF mode is similar to the FF mode, except for the longer integration time due to a number of wait states after the readout of each quadrant. Due to the long integration time it is affected by pile-up in the case of bright sources, which causes a loss of single pixel events and a gain of double pixel events at higher energies.

The ratio of readout and integration time is smaller for the eFF mode than for FF mode and thus out-of-time events are reduced which causes narrower lines. Note, that the Ni-Kα line is weaker in the LW mode as the "bright" regions (at CAMEX and TIMEX chips) are not read-out in this mode.

To visualize the effect of spatial background inhomogeneities (noise as well as excited X-rays) on pattern distributions we divided each CCD into bins of 20 pixels along the readout direction, labeled from Y0 at the CAMEX to Y9 at the center of the detector. In Fig.7 for 8 out of the 10 strips (selected over all 12 CCDs) the pattern distributions are shown with Y0 at the lower left panel, increasing CAMEX distance to the bottom, Y4 at the top of the right panels increasing down to Y9 position. The most prominent features are the increased numbers of doubles and invalid patterns close to the CAMEX while the singles noise peak is slightly shifted to higher energies due to CTI correction. A significant part of the invalid patterns is a combination of a valid event with a neighbouring noise event which can yield event patterns that cannot be caused by a single photon.

Events in the SW mode are only read out in a 64×64 CCD pixel window in CCD 4. After integration the window is shifted fast by 136 rows and then is slowly read out similar to in the Full Frame mode. We therefore can compare the SW mode distributions with the ones obtained by extracting the same window from FF mode data (Fig.8). It can be seen that the distributions are significantly different as far as the distribution of invalid patterns is concerned.

In the fast modes (TI, BU) it is assumed in the CTI correction routines that all events originate from a single `RAWY` position, as there is no spatial information along the readout direction anymore (but a fine-time coordinate). This assumption is not fulfilled here, therefore deviations from the model are expected.

5. TEMPORAL EFFECTS

The coverage of "Closed" filter observations over the 3 years of operation in orbit is only sparse. As was shown above also "CalClosed" filter exposures can be used to study the background above the Mn-Kβ line. Figure 9 combines the effect of varying background with the decay of the internal calibration source. An early observation, performed under low-background conditions, shows more soft continuum and Al and Mn line emission than a later "CalClosed" exposure under high-background conditions. At higher energies the latter one is a factor of $3-4$ brighter. This can be understood in terms of the decay of the ^{55}Fe source with ($T_{1/2} \sim 2.7$a). The right panel of Fig.9 focuses on this specific subject. For all imaging modes it shows the rate of the Mn-Kα line in the SW mode window in CCD4. Intensity variations due to out-of-time events are not corrected for, therefore the various mode curves appear to be offset.

Figure 10 summarizes the relations of the $10-12$ keV count rates versus time and versus "Discarded Line Counter" (`NDISCLIN`) which is a measure for incoming high-energy particles. From Rev. 200 on a slight increase is seen (top) while the smaller `NDISCLIN` values (blue) are due to setup changes in Rev. 223. This can be seen both in FF mode (left) and eFF mode (right panel). However, the scatter in the data is strong so that no clear correlation is evident.

6. SUMMARY AND CONCLUSIONS

The internal background of the EPIC-pn camera in the $2-7$ keV range is about 10^{-1} cts s^{-1} keV^{-1}. At higher energies this background becomes comparable to the sky background. Removing the circuit board from the sensitive volume and a graded shielding will enable to reduce this component in future X-ray instrumentation. As astrophysical interesting lines are merely at lower energies than the background fluorescence lines these in turn could be used a monitor of the line positions at high energies in science observations - in contrast to the internal calibration source where the filter wheel is in a closed position.

The fluorescence lines of Ni, Cu, and Mo show strong spatial variations correlated with camera structures, while Ti/Cr/Fe and Zn are only marginally inhomogeneous. The Al line appears to be homogeneous as aluminum is abundant in the camera.

Event pattern fractions depend on detector position (different position along readout direction for same mode), and instrument mode (same detector region but SW/FF difference) and are also energy-dependent - these quantities enter the normalization of the response files and are stored in the quantum efficiency calibration files.

The "discarded line counter" time series is affected by instrument setup changes and changes in the mission planing policies. It is used as exposure correction.

The rate of the internal calibration source has dropped by more than a factor of 2 and therefore longer monitoring observations will be needed to get sufficient statistics in one exposure.

ACKNOWLEDGMENTS

The XMM-Newton project is an ESA Science Mission with instruments and contributions directly funded by ESA Member States and the USA (NASA). The XMM-Newton project is supported by the Bundesministerium für Bildung und Forschung/Deutsches Zentrum für Luft- und Raumfahrt (BMBF/DLR), the Max-Planck-Gesellschaft, and the Heidenhain-Stiftung.

REFERENCES

1. U. G. Briel, K. Dennerl, M. Freyberg, F. Haberl, and V. E. Zavlin, "Status of the calibration of the EPIC-pn camera onboard XMM-Newton," in *X-Ray and Gamma-Ray Instrumentation for Astronomy XIII*, K. A. Flanagan and O. H. Siegmund, eds., *Proc. SPIE* **5165**, in press, 2003.
2. L. Strüder, U. Briel, K. Dennerl, R. Hartmann, and E. Kendziorra et al., "The European Photon Imaging Camera on XMM-Newton: the pn-CCD camera," *Astron. & Astrophys* **365**, pp. L18–L26, 2001.
3. F. Jansen, D. Lumb, B. Altieri, J. Clavel, and M. Ehle et al., "XMM-Newton observatory: I. the spacecraft and operations," *Astron. & Astrophys* **365**, pp. L1–L6, 2001.
4. F. Haberl, M. Freyberg, U. G. Briel, K. Dennerl, and V. E. Zavlin, "The spectral response of the EPIC-pn camera on board XMM-Newton," in *X-Ray and Gamma-Ray Instrumentation for Astronomy XIII*, K. A. Flanagan and O. H. Siegmund, eds., *Proc. SPIE* **5165**, in press, 2003.
5. M. J. Freyberg, E. Pfeffermann, and U. G. Briel, "The XMM-Newton EPIC pn camera: spatial distribution of the internal background fluorescence lines," in *New Visions of the X-ray Universe in the XMM-Newton and Chandra Era*, F. J. Jansen et al., ed., *ESA-SP* **488**, 2003 (in press, ftp://ftp.xray.mpe.mpg.de/people/mjf/mfreyberg-WA2-7.ps.gz).
6. M. J. Freyberg, U. G. Briel, K. Dennerl, F. Haberl, G. Hartner, E. Pfeffermann, E. Kendziorra, and M. Kirsch, "The XMM-Newton EPIC pn camera: spectral and temporal properties of the internal background," in *New Visions of the X-ray Universe in the XMM-Newton and Chandra Era*, F. J. Jansen et al., ed., *ESA-SP* **488**, 2003 (in press, ftp://ftp.xray.mpe.mpg.de/people/mjf/mfreyberg-WA2-16.ps.gz).
7. K. Dennerl, U. G. Briel, F. Haberl, G. Hartner, N. Krause, and V. E. Zavlin, "Determination and correction of the charge transfer efficiency of the pn-CCD camera," in *X-Ray and Gamma-Ray Instrumentation for Astronomy X*, O. H. Siegmund and K. A. Flanagan, eds., *Proc. SPIE* **3765**, pp. 232–243, 1999.
8. B. Aschenbach, U. G. Briel, F. Haberl, H. Bräuninger, W. Burkert, A. Oppitz, P. Gondoin, and D. Lumb, "Imaging performance of the XMM-Newton x-ray telescopes," in *X-Ray Optics, Instruments, and Missions III*, J. E. Trümper and B. Aschenbach, eds., *Proc. SPIE* **4012**, pp. 731–739, 2000.
9. M. J. Freyberg and D. Breitschwerdt, "XMM-Newton local bubble and galactic halo survey," *Astron. Nachr.* **324**, p. 162, 2003.
10. U. G. Briel, H. Bräuninger, K. Dennerl, C. Greiveldinger, and F. Haberl et al., "Calibration and preliminary results on the performance of the XMM EPIC pn flight camera: imaging modes," in *EUV, X-Rays and Gamma-Ray Instrumentation for Astronomy IX*, O. H. Siegmund and K. A. Flanagan, eds., *Proc. SPIE* **3445**, pp. 38–49, 1998.

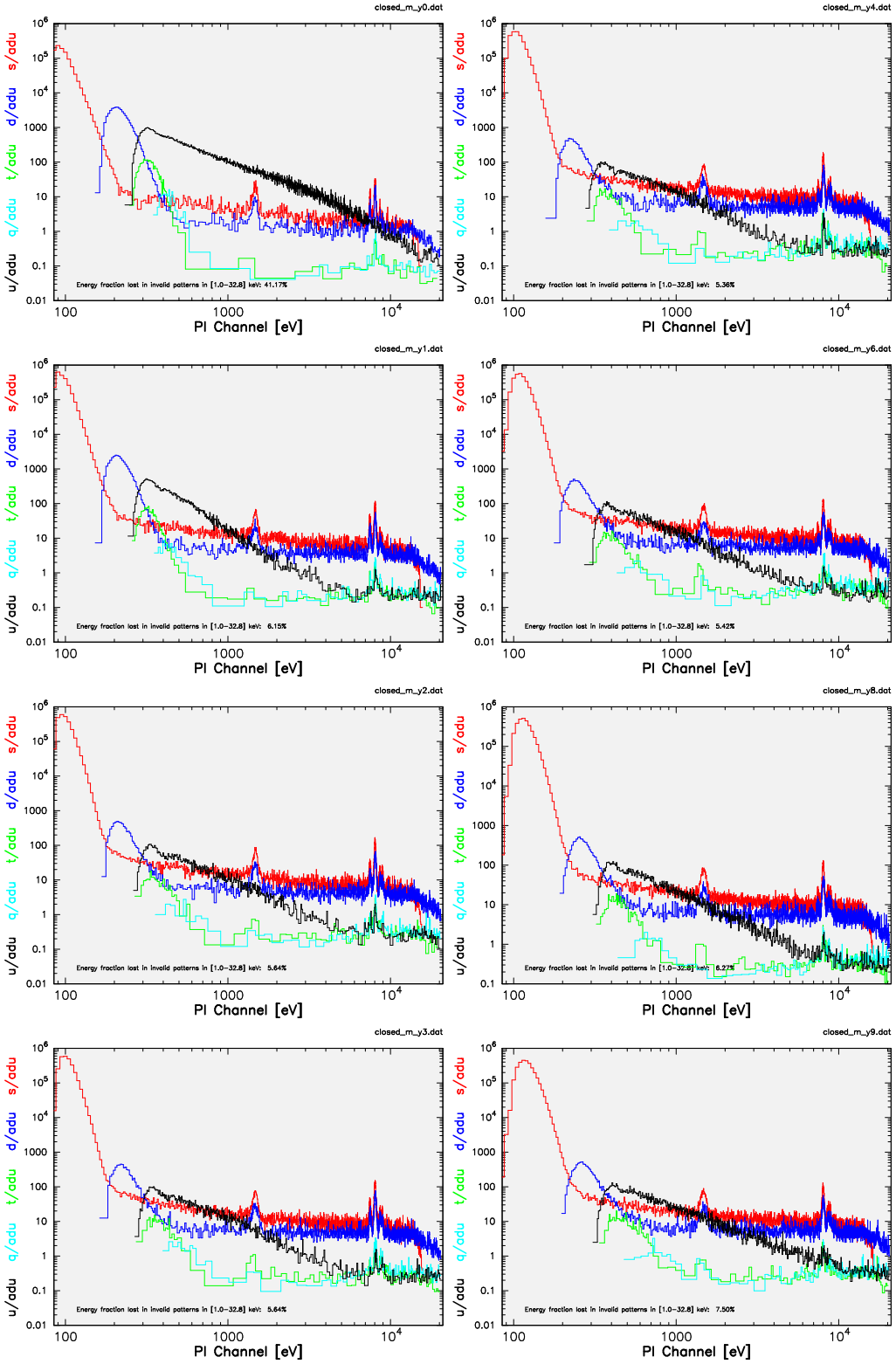

Figure 7. Event pattern distributions for merged FF mode "Closed" filter data, positions Y0,1,2,3 (left) and 4,6,8,9 (right), corresponding to increasing distance to the CAMEX. For details see text.

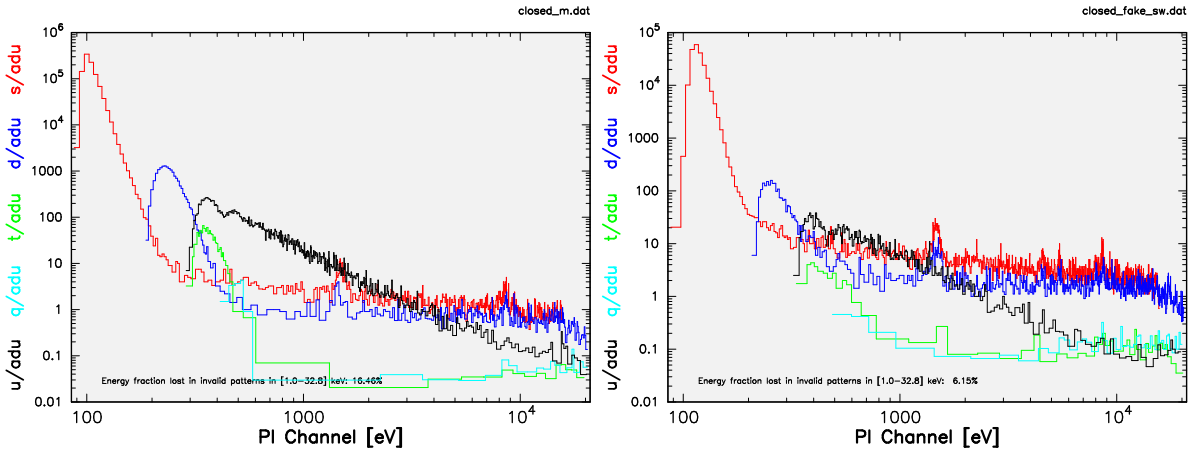

Figure 8. Event pattern distributions for SW mode (left) and for FF mode where only the SW mode window has been extracted (right panel). The different absolute normalization is due to factor of 3 shorter SW mode exposure times. In SW mode there are significantly more invalid patterns relative to single events compared to the same CCD region in FF mode.

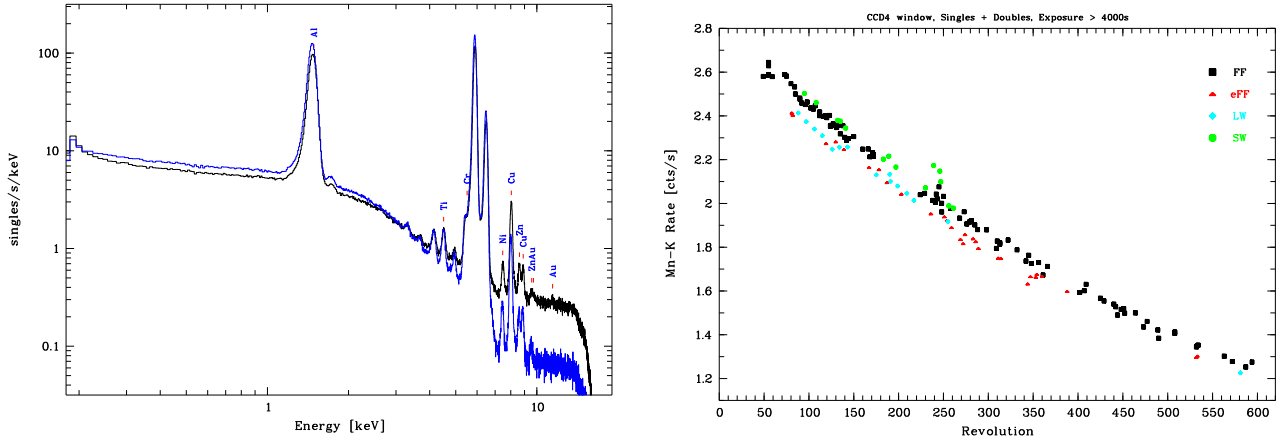

Figure 9. In the left panel a low-background "CalClosed" (Rev.80, 16-May-2000, blue) observation is compared with a high-background "CalClosed" (Rev.242, 4-Apr-2001, black) exposure, with only single events selected. The time lag between the exposures is ~ 0.88 a. The weakening in the Al and Mn lines and also in the low-energy continuum is due to the decay of the ^{55}Fe source ($T_{1/2} \sim 2.7$a), the increase mostly visible above ~ 7 keV is caused by excessively high particle radiation. This weakening is also illustrated in the right panel, where for the various imaging modes the count rate of the ^{55}Fe source in the SW mode window is shown as a function of time.

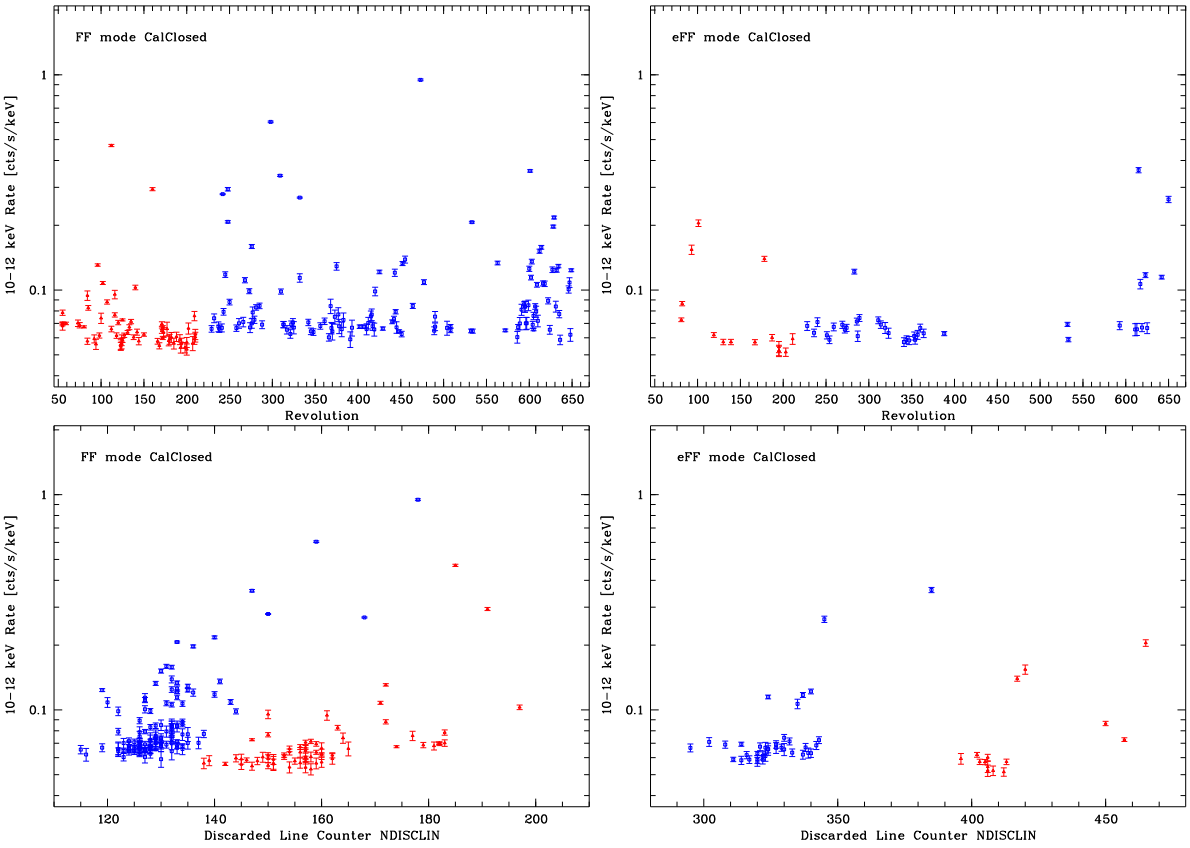

Figure 10. Lightcurves of the $10-12$ keV single-pixel rates in "CalClosed" FF mode (left) and eFF mode data (right), the same intensities plotted versus the corresponding average "Discarded Line Counter" NDISCLIN (bottom panels, without Revs. 248 and 309). The EPEA setup was changed during the mission, red triangles denote data points before and blue squares after the change, respectively. Therefore NDISCLIN is only a measure for a certain setup (and instrument mode due to different integration times as basis for the MIP rejection). Additionally, the mission planning was changed, "CalClosed" filter exposures were scheduled at the beginning of a revolution where the background level is generally higher, or too high for scientific observations.